

A Cavity of Large Grains in the Disk Around the Group II Herbig Ae/Be Star HD 142666

A. E. Rubinstein¹, E. Macías², C. C. Espaillat², K. Zhang¹, N. Calvet¹, C. Robinson²

¹ *Department of Astronomy, University of Michigan, Ann Arbor, MI 48109, USA*

² *Department of Astronomy, Boston University, 725 Commonwealth Avenue, Boston, MA 02215, USA*

ABSTRACT

Herbig Ae/Be (HAeBe) stars have been classified into Group I or Group II, which were initially thought to be flared and flat disks, respectively. Several Group I sources have been shown to have large gaps, suggesting ongoing planet formation, while no large gaps have been found in the disks of Group II sources. We analyzed the disk around the Group II source, HD 142666, using irradiated accretion disk modeling of the broad-band spectral energy distribution along with the 1.3 millimeter spatial brightness distribution traced by Atacama Large Millimeter and Submillimeter Array (ALMA) observations. Our model reproduces the available data, predicting a high degree of dust settling in the disk, which is consistent with the Group II classification of HD 142666. In addition, the observed visibilities and synthesized image could only be reproduced when including a depletion of large grains out to ~ 16 au in our disk model, although the ALMA observations did not have enough angular resolution to fully resolve the inner parts of the disk. These results may suggest that some disks around Group II HAeBe stars have cavities of large grains as well. Further ALMA observations of Group II sources are needed to discern how commonly cavities occur in this class of objects, as well as to reveal their possible origins.

Subject headings: accretion, accretion disks — planets and satellites: formation — protoplanetary disks — stars: individual (HD 142666) — stars: pre-main sequence — techniques: interferometric

1. Introduction

Protoplanetary disks have long been thought to be the birthplaces of planetary systems. Early models of dust evolution predicted that the dust inherited from the ISM grew by colliding, sticking together, and settling towards the disk midplane, where further interactions made them grow towards planetesimals and planets (Weidenschilling 1997). Observations have supported and expanded this view; in particular, they have revealed disk structures that have been attributed to interactions between the disk and forming planets (cf. Espaillat et al. 2014).

Before the advent of high-spatial resolution instruments, disk properties were often inferred from studies of the spectral energy distributions (SEDs) of young objects. In particular, such studies have focused on young, intermediate-mass stars, known as Herbig Ae/Be stars (HAeBe) (Waters &

Waelkens 1998), which have been separated into two groups, Group I and Group II. This classification came from fitting the mid-IR ($15 - 45 \mu\text{m}$) portion of HAeBe stars' SEDs. The SEDs of Group I stars required both a blackbody and power law to fit, while those of Group II stars could be fit with only a power law (Meeus et al. 2001). On average, it was noted that Group I stars have larger IR excesses when compared with Group II stars (Dominik et al. 2003), which has been quantified by using IRAS (van Boekel et al. 2003) and Herschel data (Pascual et al. 2016). Specifically, the latter study found that Group II sources have a lower ratio of far-IR ($20 - 200 \mu\text{m}$) to near-IR ($2 - 5 \mu\text{m}$) flux than do Group I sources. In turn, these differences have been interpreted as Group I objects having “flared” disks and Group II objects having “flat” disks. Flared disks are defined such that the height of the disk increases rapidly with radius, capturing more stellar light,

and therefore being hotter (Kenyon & Hartmann 1987) than flat disks. In fact, flared, Group I sources were thought to evolve into flatter, Group II sources due to dust growth and settling (Dullemond & Dominik 2004).

However, further differences were found that brought into question the evolutionary relationship between the groups. SED modeling ($\sim 0.1 - 1000 \mu\text{m}$), together with N-band, Q-band, and $25 \mu\text{m}$ imaging, revealed that many Group I sources have large, >20 au, inner gaps or cavities (e.g., Maaskant et al. 2013; Honda et al. 2015). In contrast, based on N-band interferometry, Group II sources have only showed evidence of smaller, <1 au gaps close to the dust sublimation radius (e.g. HD 142666, HD 144432; Menu et al. 2015).

The Atacama Large Millimeter and Submillimeter Array (ALMA) has provided images of protoplanetary disks with extreme detail, revealing substructures, such as narrow gaps and rings, that could not previously be studied (ALMA Partnership et al. 2015; Andrews et al. 2016). For Group II sources, prior ALMA observations have often focused on the disk’s chemical content, gas dynamics, or disk asymmetries instead of substructures like gaps or cavities (Guzmán et al. 2015; Czekala et al. 2015; White et al. 2018; Kataoka et al. 2016). Recently, though, ALMA observations revealed shallow, >20 au gaps around the Group II source HD 163296 (Isella et al. 2016; Zhang et al. 2016; Muro-Arena et al. 2018), suggesting the possible presence of gaps or cavities in other Group II sources.

Here, we study the Group II H Ae star HD 142666 (V1026 Sco, Meeus et al. 2001), located in the Upper Sco OB-2 association (Sandell et al. 2011; $d=150.1$ pc; Gaia Collaboration et al. 2016a). HD 142666 has been observed from near-IR wavelengths, detecting the scattered light from the disk (Garufi et al. 2017), to sub-mm wavelengths, detecting the unresolved emission from the $^{12}\text{CO } J = 2 - 1$ (Panić & Hogerheijde 2009) and $^{12}\text{CO } J = 3 - 2$ (Dent et al. 2005) rotational lines.

Some structure has also been found in the disk of HD 142666. From SED modeling and interferometric observations in the $1.6 - 2.5 \mu\text{m}$ and $8 - 13 \mu\text{m}$ wavelength ranges, Schegerer et al. (2013) inferred the existence of a hole in the disk inside 0.3 au and a dust-free gap between 0.35 au and

0.8 au. On the other hand, Banzatti et al. (2018) found evidence for no or a very small cavity for this disk in their study combining near-IR ($1.2 - 4.5 \mu\text{m}$) and CO rovibrational emission. So far, no evidence has suggested the presence of a large gap or cavity around HD 142666 comparable to those found in Group I sources.

In this paper, we present a physically self-consistent model of the SED and ALMA observations for the disk around HD 142666. In Section 2.1, we describe the archival photometry and spectra used for the SED modeling. In Section 2.2, we present archival 1.3 mm (Band 6) ALMA observations, and we show the results of an initial analytical fit to the observations. In Section 3.1, we describe the model and physical parameters used to reproduce the observations. In Section 3.2, we summarize the results, including a cavity extending radially out to ~ 16 au in the disk’s large dust grain distribution. Finally, in Section 4, we put this large cavity in context with relevant results involving cavities and gaps in HAeBe disks.

2. Observations and Results

2.1. Stellar Properties and the SED

To construct the SED of HD 142666 and its disk (Figure 1), we gathered the IRS spectrum (Keller et al. 2008) and visible to mm photometry from 2MASS, AKARI, IRAS, Tycho-2, WISE, and van der Veen et al. (1994); Sylvester et al. (1996); Malfait et al. (1998); Natta et al. (2004); Meeus et al. (2012); Mendigutía et al. (2012) and Pascual et al. (2016). We note that we did not include photometry that overlapped with the IRS wavelengths (e.g. From AKARI or WISE) in order to avoid the wide bandpasses of these filters.

The data was dereddened using the Mathis (1990) reddening law by first finding the extinction $E(B-V)$ from the observed B-V color and the intrinsic $(B-V)_0$ color from Kenyon & Hartmann (1995). Assuming $R_V = 3.1$, we obtained $A_V = 0.992$. The stellar luminosity was then derived using the dereddened V-band magnitude. This luminosity, together with the effective temperature, was compared with evolutionary tracks (Siess et al. 2000) to obtain a stellar mass. These stellar properties are shown in Table 1.

The mass accretion rate (\dot{M}) for HD 142666 has been measured to be between 1×10^{-8} and $2 \times$

$10^{-7} M_{\odot} \text{ yr}^{-1}$ (Salyk et al. 2013; Mendigutía et al. 2011; Donehew & Brittain 2011; Garcia Lopez et al. 2006). Even though the range in these measurements could be due to intrinsic variability, these papers used different methods, making comparison difficult.

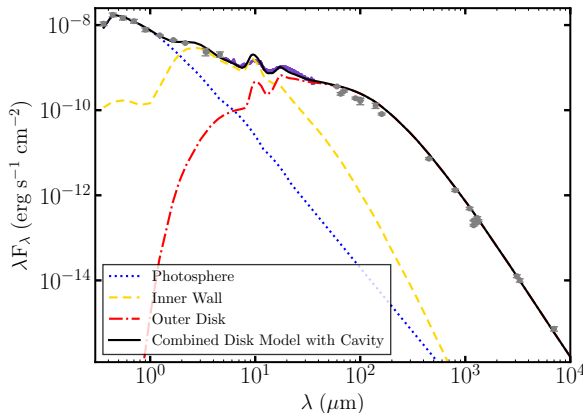


Fig. 1.— The SED including photometric data (gray dots) and the IRS spectrum (purple dots). The black curve shows the disk model including a cavity that fits the observations. Other curves represent contributions (i.e. from the star or disk) that are added to produce this model.

2.2. ALMA Observations

We used Cycle 2 ALMA archival observations (PI: L. Pérez) of the protoplanetary disk of HD 142666. The data were calibrated using the reduction package Common Astronomy Software Applications (CASA; McMullin et al. 2007). HD 142666 was observed on July 21, 2015 at Band 6 using an array of 44 antennas. The observations were flux calibrated with the QSOs J1517-2422 and J1627-2426 and bandpass calibrated with Titan. The total on-source time was 59.04 minutes. Two spectral windows (SPW) centered at 216.974 and 232.349 GHz were used to detect the continuum, each with a bandwidth of 1.875 GHz.

We used the CLEAN task in CASA interactively to obtain deconvolved images from the observed visibilities. We chose a uniform weighting, resulting in a synthesized beam of $0''.200 \times 0''.165$ and an rms sensitivity of $0.22 \text{ mJy beam}^{-1}$. The lower left panel of Figure 2 shows the resulting 1.38 mm continuum image. The continuum emission

shows a resolved, compact disk without apparent evidence of non-axisymmetry or a gap.

Enclosing the source inside a $1'' \times 1''$ box, we estimated a flux density of $113 \pm 6 \text{ mJy}$, consistent with the results of a Gaussian fit to the image. The Gaussian fit was also used to estimate the central coordinates, position angle (PA; 161°), FWHM (30 au), and inclination ($\sim 60^\circ$) of the disk.

Finally, we changed the phase center and deprojected the visibilities using small shifts in position, as well as different values of inclination and PA. The values that resulted in the minimum scatter in the real and imaginary parts of the visibilities were consistent with the results found by the Gaussian fit. The measured inclination agrees with previous studies based on H-band interferometric observations (Lazareff et al. 2017) and modeling of mid-IR interferometry (Vural et al. 2014).

In Figure 3, we show the deprojected, real part of the visibilities. We note that the ALMA continuum observations are split into two SPWs that are separated by $\sim 15 \text{ GHz}$ but have a high SNR individually. Thus, we have analyzed both SPWs separately and only show the results for the SPW centered at 216.974 GHz (1.38 mm). The visibilities show a very steep decrease followed by a null at $\sim 500 \text{ k}\lambda$, suggesting the presence of a cavity in the disk (Hughes et al. 2007). To characterize the disk’s intensity profile, we fit the visibilities using a parametric model of the surface brightness profile of the disk as in Zhang et al. (2016). The top panels of Figure 3 show the results of this modeling. The resulting intensity profile shows a drop in intensity at $R < 9.5 \text{ au}$. We used this intensity profile as a first estimate for the following physical disk modeling.

3. Modeling

3.1. Modeling Procedure

We modeled the SED and ALMA continuum observations of HD 142666 using the physically self-consistent disk model by D’Alessio et al. (2006). The model computes the radial and vertical structure of an irradiated accretion disk while also enforcing hydrostatic equilibrium. It includes a wall at the inner edge of the disk that is directly irradiated by the star. In addition, we added a tapered edge to the disk’s surface density profile

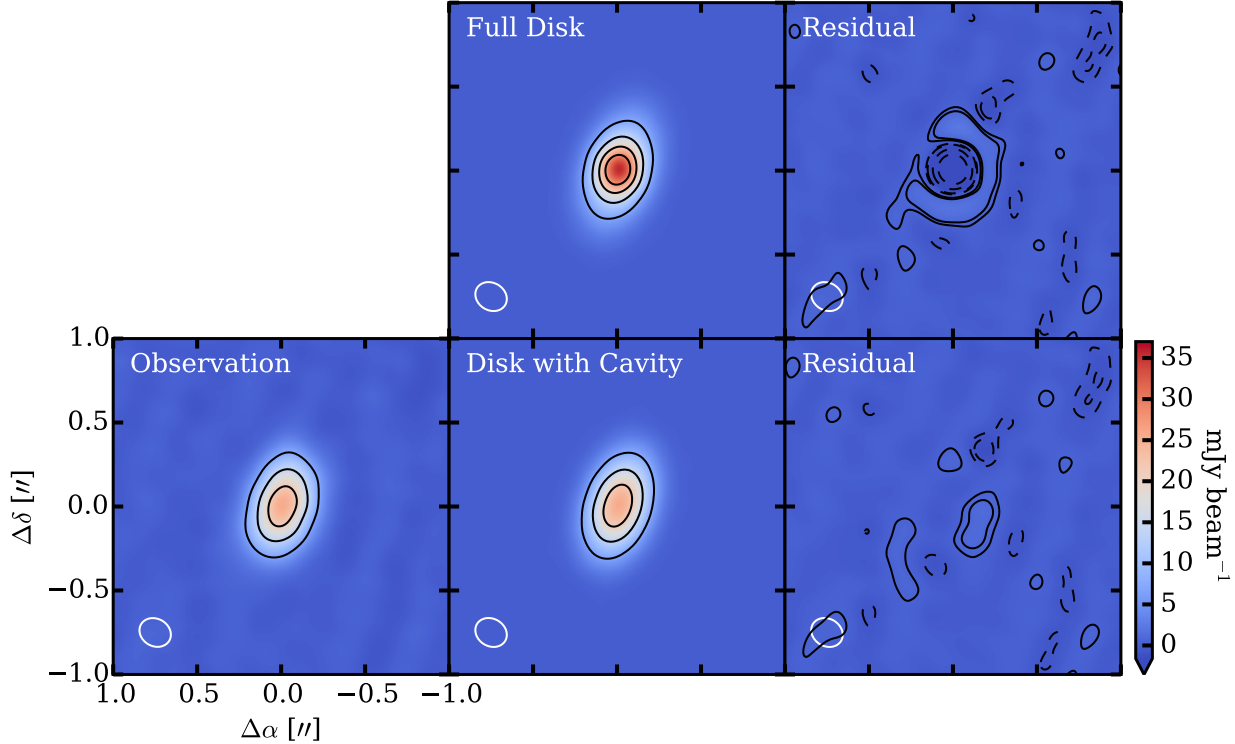


Fig. 2.— The synthesized ALMA continuum image of HD 142666 at 1.38 mm (bottom left), along with the simulated model image from a full disk (center, top) and a cavity-containing disk (center, bottom), and the residual images produced from subtracting the observed and model visibilities (right of the respective simulated image). The ellipse in the lower left corner shows the beamsize. The contours for the observation and cavity-containing disk model are 0.2, 0.4, 0.6, 0.8 times the maximum brightness of the image. The contours for the residual are ± 3 , ± 5 , ± 15 , ± 30 times the rms of the image, $170 \mu\text{Jy/beam}$.

following $e^{-(R/R_d)^\gamma}$, where R_d is the outer disk radius at which the tapering begins, and γ determines its steepness. The viscosity is described by the parameter α following Shakura & Sunyaev (1973). We left it fixed because of its degeneracy with \dot{M} (D’Alessio et al. 2006). The dust in the disk was described by two populations of grains with size distributions $n(a) \propto a^{-3.5}$ between a minimum size, $a_{\min} = 0.005 \mu\text{m}$, and maximum size, a_{\max} , which was kept as a free parameter. The large grains (a_{\max}^{mid}) were concentrated at the midplane of the disk, while the small grains (a_{\max}^{atm}) were located mostly in the upper layers (D’Alessio et al. 2006). To include dust settling, the population of small grains in the disk atmosphere was depleted by a factor ϵ , which is the ratio of the dust-to-gas mass ratio of small grains to the standard dust-to-gas mass ratio. The dust-to-gas

mass ratio of the large grains in the midplane was increased to conserve the standard mass ratio at each radius (D’Alessio et al. 2006). The wall emission was calculated following D’Alessio et al. (2005). The maximum grain size in the wall at the dust destruction radius, as well as the dust sublimation temperature, T_{wall} , and the height of the wall, z_{wall} , were kept as free parameters.

Following the results of the parametric model of the surface brightness profile (Section 2.2), we also included a cavity in the distribution of large dust grains in some models. Here, we define “cavity” as a region of the disk in which dust is significantly depleted. We note that the near-IR and mid-IR parts of the SED, which traced the small dust grains located close to the star, did not show significant depletion. Therefore, we included an

TABLE 1
STELLAR PROPERTIES

Sp. Type	T _{eff} (K)	A _V	L (L _⊙)	M (M _⊙)	R (R _⊙)
A8	7580	0.992	14.3	2.0	2.2

NOTE.—We adopt a spectral type of A8 spectral type from Mora et al. (2001) and a T_{eff} of 7580 K following Kenyon & Hartmann (1995).

inner cavity in our model by decreasing the abundance of only the large grains out to R_{cav} by a factor δ_{cav} .

We considered combinations of parameters using a grid of disk models. The range of values explored are shown in Table 2. The inclination, i , and R_d of the disk were initially constrained using the ALMA observations (Section 2.2). From the grid of parameters tested, the models that best fit the SED were obtained by minimizing the χ^2 . A synthetic image of each model was computed. The images were then Fourier transformed and sampled with the uv coverage of the ALMA observations, obtaining the simulated visibilities of the model. From these visibilities, an image was obtained using the CLEAN task in CASA. The simulated visibilities and images were compared with the observed visibilities and the averaged radial profile of the disk, respectively.

3.2. Disk Properties

Figure 1 shows the final fit to the SED, and Figure 2 shows the model (middle) and residual (right) images. The fit to the real part of the visibilities and to the radial profiles are shown in the lower panels of Figure 3. The parameters that best fit the SED and ALMA observations are shown in Table 2.

Full disk models always failed to reproduce the visibilities and the inner parts of the radial profile (Figures 2 and 3). We found our best fit to the ALMA observations when including a cavity in the large dust grains out to 15.6 au. Nevertheless, the near-IR and mid-IR range of the SED fit

well with a continuous abundance of small grains, suggesting that small dust grains are filling the cavity.

Our best fit also corresponded to an inner edge of the disk (R_{wall}) of 1.3 au (Table 2). In comparison, Schegerer et al. (2013) and Vural et al. (2014), obtained inner disk radii of 0.8 au and 1.35 au, respectively. These studies found additional structure inside these radii using near-IR and mid-IR visibilities. We do not attempt to include these constraints in this paper. However, since near-IR emission arises in small dust in the atmospheric layers of the inner disk (D’Alessio et al. 2006), the Schegerer et al. (2013) and Vural et al. (2014) results are consistent with having small dust down to scales ~ 1 au, in agreement with our results.

To find the dust mass of the disk, we integrated the surface density distribution of our best fit disk model and found a mass of $5.3 \times 10^{-4} M_{\odot}$. Assuming a dust-to-gas mass ratio of 0.01, we then found a total disk mass of $0.0533 M_{\odot}$ and a mass of $1.55 \times 10^{-7} M_{\odot}$ for small grains in the disk’s cavity. We also found a high degree of settling in the disk ($\epsilon = 0.001$), which was consistent with the classification of HD 142666 as a Group II source. As indicated by the ALMA observations, the disk of HD 142666 is also fairly compact, with an R_d of 65 au and a relatively sharp edge.

4. Discussion

From the results of our physical irradiated accretion disk model, we have inferred the presence of a cavity in large dust grains out to 15.6 au in the

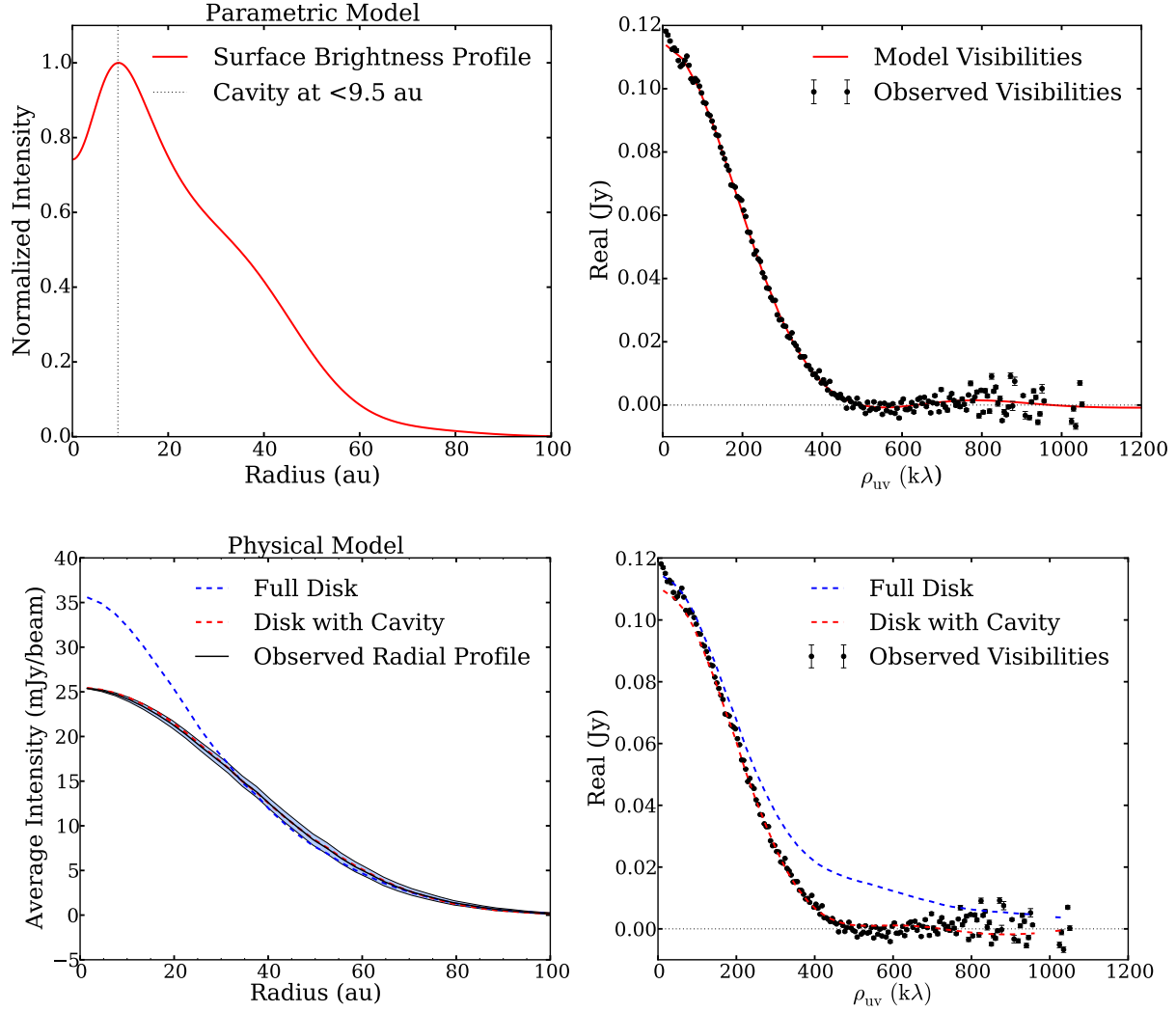


Fig. 3.— *Top* – Results from our parametric model of the surface brightness profile of the disk. The normalized surface brightness profile of the best-fit model is shown on the left. The vertical line indicates the edge of a shallow cavity at <9.5 au. The right panel shows the observed (black dots) and model (red line) visibilities. *Bottom* – Results from our physical disk model. On the left panel, we show the averaged radial intensity profile of the observed image (black line), and of the simulated ALMA image obtained from the disk model (dashed lines). The error bars for the observed radial profile are computed based on the standard deviation of the disk emission at each radius. We note that the inner cavity is not clearly seen in the radial profile because of the angular resolution of the observations (~ 30 au). The observed (black dots) and model (dashed lines) visibilities are plotted on the right. The blue and red lines indicate the best-fit models using a full disk and a disk with a cavity of large grains, respectively. Based on the visibilities and the radial intensity profiles, the observations can only be fit when including an inner cavity in the disk.

TABLE 2
MODEL PROPERTIES

Parameter	Range of Parameters Tested	Best Fit
Wall		
a_{\max} (μm)	0.1 – 100	1
R_{wall} (au)	...	1.3
T_{wall} (K)	1000 – 1500	1100
z_{wall} (au)	0.27 – 0.4	0.32
Cavity		
δ_{cav}	1 – 0.001	0.11
R_{cav} (au)	8 – 20	15.6
Disk		
a_{\max}^{atm} (μm)	0.1 – 100	2
a_{\max}^{mid} (cm)	0.1 – 1	1
α	0.01	0.01
ϵ	0.001 – 1	0.001
i ($^{\circ}$)	40 – 70	60
\dot{M} ($M_{\odot} \text{ yr}^{-1}$)	$1 \times 10^{-8} - 2 \times 10^{-7}$	7.5×10^{-8}
R_{d} (au)	30 – 100	65
γ	1 – 10	8

NOTE.—The radius of the wall, R_{wall} , follows from the temperature of the wall, T_{wall} , following D’Alessio et al. (2005).

disk of HD 142666. These results are supported by the parametric model, based on the surface brightness profile, that fits the deprojected visibilities and indicates a significant decrease of mm emission at $R < 9.5$ au. Our results are the first evidence of the presence of a wider cavity of large grains in the disk, which may have been elusive in the past because it is present only in the large dust grain distribution traced by the ALMA observations. Group II sources have been proposed to have their outer disks self-shadowed by the inner regions of the disk, which could result in a colder, ring-like region of the disk. Nevertheless, this cannot explain the cavity revealed by the ALMA observations since the radio emission probes dust in the midplane, where a shadow would have a very small effect.

Several mechanisms have been proposed to explain the presence of cavities in protoplanetary disks (Espaillat et al. 2014). One mechanism involves dynamical interactions due to planets in the disk, which have been shown to open cavities and gaps in the dust distribution. Additionally, the edges of these cavities represent local pressure maxima, which can trap large dust grains, while allowing small dust grains to move towards the star and fill the cavity (Zhu & Stone 2014). Thus, since the cavity in HD 142666’s disk is present mainly in the large dust grain distribution, this cavity aligns with a planetary origin.

We compare the dust distribution of HD 142666 with that of the Group I object HD 100546. ALMA observations reveal ~ 10 au cavities in the large grains in both objects (this work; HD 100546, Pineda et al. 2014). The largest difference is in the distribution of small grains. In HD 100546, small grains populate the disk at radii < 1 au, producing near-IR excess. Small grains also coexist with large grains in the outer disk. But a large region, between ~ 1 au and ~ 10 au, is essentially depopulated of small grains (based on AMBER/MIDI; Benisty et al. 2010). In contrast, there is no such large gap in the small grains in the disk of HD 142666; they are present in the disk down to ~ 1 au (based on AMBER/MIDI; Schegerer et al. 2013; Vural et al. 2014).

More generally, prior studies in the near-IR to mid-IR showed that most Group I sources have large, > 20 au, inner clearings of dust (Maaskant et al. 2013; Honda et al. 2015), while cavities

found in Group II sources have been small, < 1 au, and detected only close to the sublimation radius (Menu et al. 2015). Together with the proposed structural differences between the disks of Group I and Group II sources as indicated by their SEDs, these different cavities and structures have been explained with two scenarios: different evolutionary stages (a common ancestry) or separate evolutionary paths (Maaskant et al. 2013; Menu et al. 2015; Garufi et al. 2017). Garufi et al. (2017) postulated that as gaps are only present in the disks of Group I sources, the groups were more likely to evolve along separate paths.

Our results have showed that HD 142666 has an inner cavity extending out to ~ 15.6 au. In addition, the Group II source HD 163296 was recently shown to have multiple gaps, as well as a possible shallow, inner gap with a width of ~ 20 au (Muro-Arena et al. 2018; Zhang et al. 2016; Isella et al. 2016). Although the classification of HD 163296 as Group II has been disputed by Muro-Arena et al. (2018), our results indicate that the characterization of Group I and Group II sources as gapped and continuous disks may not always apply.

The inner cavities and gaps in the disks of Group II sources, as with those of HD 142666 and HD 163296, may be smaller and/or shallower than those in the disks of Group I sources, which may also explain why inner cavities and gaps of disks around Group II sources are not evident in SEDs. In fact, the SEDs of other Group II sources set constraints on the size of inner cavities, if present. Thus, even though cavities and gaps can be present in the disks of both Group I and Group II sources, there seems to be differences in the size of cavities and gaps between the two groups. These differences cannot be explained by a scenario where Group I sources evolve into Group II sources, since inner gaps or cavities are not expected to decrease in size or to be refilled with dust during their evolution. An inverse process could be postulated, where the gaps of Group II sources get larger with time so that Group II evolves into Group I (e.g., Menu et al. 2015). However, as pointed out by Garufi et al. (2017), the fact that disks around Group II sources have lower millimeter fluxes and smaller disk sizes than those of Group I sources does not favor this possibility.

Therefore, despite having shown that gaps can

be present in disks around both Group I and Group II sources, different evolutionary tracks still seem to be the most likely scenario to explain both groups. The different gap sizes between Group I and Group II could in fact be a direct consequence of these different evolutionary tracks. If Group I includes denser and more massive disks, then they could be more likely to form giant planets. If so, such planets would open wider and deeper cavities than those around Group II sources, which, if present, would be formed by less massive planets.

In conclusion, our results, together with previous observations of HD 163296, show that the disks of Group II sources can contain cavities or gaps of large grains, despite prior claims. These inner gaps or cavities of large grains may be, however, smaller than those seen around Group I sources. Our detailed modeling of HD 142666 also indicates that no corresponding cavities exist in the small grains. Higher angular resolution observations with ALMA will be necessary to confirm whether cavities are present in the disks of other Group II sources. Such studies will inform how disk structure relates to planet formation.

5. Acknowledgments

We thank Megan Reiter, Thanawuth Thanathibodee, and Sierra Grant for useful discussions. A.E.R. is grateful for the support given by the National Science Foundation Research Experiences for Undergraduates program through NSF grant 13-542. C.C.E. acknowledges support from the Sloan foundation. K.Z. acknowledges the support of NASA through Hubble Fellowship grant HST HF2-51401.001-A awarded by the Space Telescope Science Institute, which is operated by the Association of Universities for Research in Astronomy, Inc., for NASA, under contact NAS-26555.

This research made use of the SIMBAD database, operated at the CDS, Strasbourg, France. This paper also makes use of the following ALMA data: ADS/JAO.ALMA#2013.1.00498.S. ALMA is a partnership of ESO (representing its member states), NSF (USA) and NINS (Japan), together with NRC (Canada) and NSC and ASIAA (Taiwan) and KASI (Republic of Korea), in cooperation with the Republic of Chile. The Joint ALMA Observatory is operated by ESO, AUI/NRAO and NAOJ. The National Radio Astronomy Observa-

tory is a facility of the National Science Foundation operated under cooperative agreement by Associated Universities, Inc.

REFERENCES

- ALMA Partnership, Brogan, C. L., Pérez, L. M., et al. 2015, *ApJ*, 808, L3
- Andrews, S. M., Wilner, D. J., Zhu, Z., et al. 2016, *ApJ*, 820, L40
- Banzatti, A., Garufi, A., Kama, M., et al. 2018, *A&A*, 609, L2
- Benisty, M., Tatulli, E., Ménard, F., & Swain, M. R. 2010, *A&A*, 511, A75
- Czekala, I., Andrews, S. M., Jensen, E. L. N., et al. 2015, *ApJ*, 806, 154C
- D’Alessio, P., Hartmann, L., Nuria, C., Franco-Hernández, R., et al. 2005, *ApJ*, 621, 461
- D’Alessio, P., Calvet, N., Hartmann, L., Franco-Hernández, R., & Servín, H. 2006, *ApJ*, 638, 314
- Dent, W. R. F., Greaves, J. S., & Coulson, I. M. 2005, *MNRAS*, 359, 663
- Dominik, C., Dullemond, C. P., Waters, L. B. F. M., Walch, S. 2003, *A&A*, 398, 607
- Donehew, B., & Brittain, S. 2011, *AJ*, 141, 46
- Dullemond, C. P., & Dominik, C. 2004, *A&A*, 417, 159
- Espaillet, C., Calvet, N., D’Alessio, P., et al. 2007, *ApJ*, 670, L135
- Espaillet, C., D’Alessio, P., Hernández, J., et al. 2010, *ApJ*, 717, 441
- Espaillet, C., Muzerolle, J., Najita, J., et al. 2014, *Protostars and Planets VI*, 497
- Furlan, E., Hartmann, L., Calvet, N., et al. 2006, *ApJS*, 165, 568
- Gaia Collaboration, Brown, A. G. A., Vallenari, A., et al. 2016a, *A&A*, 595, A2
- Garcia Lopez, R., Natta, A., Testi, L., & Habart, E. 2006, *A&A*, 459, 837

- Garufi, A., Quanz, S. P., Schmid, H. M., et al. 2016, *A&A*, 588, A8
- Garufi, A., Meeus, G., Benisty, M., et al. 2017, *A&A*, 603, A21
- Guzmán, V. V., Öberg, K. I., Loomis, R., & Qi, C. 2015, *ApJ*, 814, 53G
- Honda, M., Maaskant, K., Okamoto, Y. K., et al. 2015, *ApJ*, 804, 143
- Hughes, A. M., Wilner, D. J., Calvet, N., et al. 2007, *ApJ*, 664, 536
- Isella, A., Guidi, G., Testi, L., et al. 2016, *Physical Review Letters*, 117, 251101
- Kamp, I., & Dullemond, C. P. 2004, *ApJ*, 615, 991
- Kataoka, A., Tsukagoshi, T., Momose, M., et al. 2016, *ApJ*, 831, L12
- Keller, L. D., Sloan, G. C., Forrest, W. J., et al. 2008, *ApJ*, 684, 411
- Kenyon, S. J., & Hartmann, L. 1987, *ApJ*, 323, 714
- Kenyon, S. J., & Hartmann, L. 1995, *ApJS*, 101, 117
- Lazareff, B., Berger, J.-P., Kluska, J., et al. 2017, *A&A*, 599, A85
- Maaskant, K. M., Honda, M., Waters, L. B. F. M., et al. 2013, *A&A*, 555, A64
- Malfait, K., Bogaert, E., & Waelkens, C. 1998, *A&A*, 331, 211M
- Mathis, J. S. 1990, *ARA&A*, 28, 37
- McClure, M. K., Furlan, E., Manoj, P., et al. 2010, *ApJS*, 188, 75
- McMullin, J. P., Waters, B., Schiebel, D., Young, W., & Golap, K. 2007, in *Astronomical Society of the Pacific Conference Series*, Vol. 376, *Astronomical Data Analysis Software and Systems XVI*, ed. R. A. Shaw, F. Hill, & D. J. Bell, 127
- Meeus, G., Waters, L. B. F. M., Bouwman, J., et al. 2001, *A&A*, 365, 476
- Meeus, G., Montesinos, B., Mendigutía, I., et al. 2012, *A&A*, 544, A78
- Mendigutía, I., Calvet, N., Montesinos, B., et al. 2011, *A&A*, 535, A99
- Mendigutía, I., Mora, A., Montesinos, B., et al. 2012, *A&A*, 543, A59
- Menu, J., van Boekel, R., Henning, T., et al. 2015, *A&A*, 581, A107
- Mora, A., Merín, B., Solano, E., et al. 2001, *A&A*, 378, 116
- Muro-Arena, G. A. and Dominik, C. and Waters, L. B. F. M., et al. 2018, *A&A*
- Natta, A., Testi, L., Neri, R., et al. 2004, *A&A*, 416, 179N
- Panić, O., & Hogerheijde, M. R. 2009, *A&A*, 508, 707
- Pascual, N., Montesinos, B., Meeus, G., et al. 2016, *A&A*, 586A, 6P
- Pineda, J. E., Quanz, S. P., Meru, F., et al. 2014, *ApJ*, 788, L34
- Salyk, C., Herczeg, G. J., Brown, J. M., et al. 2013, *ApJ*, 769, 21
- Sandell, G., Weintraub, D. A., & Hamidouche, M. 2011, *ApJ*, 727, 26
- Scheegerer, A. A., Ratzka, T., Schuller, P. A., et al. 2013, *A&A*, 555, A103
- Siess, L., Dufour, E., & Forestini, M. 2000, *A&A*, 358, 593
- Shakura, N. I. & Sunyaev, R. A. 1973, *A&A*, 24, 337
- Sylvester, R. J., Skinner, C. J., Barlow, M. J. & Mannings, V. 1996, *MNRAS*, 279, 915
- van Boekel, W. E. C. J., Waters, L. B. F. M., Trams, N. R., Matthews, H. E. 2003, *A&A*, 400, L21
- van der Veen, W. E. C. J., Waters, L. B. F. M., Trams, N. R., Matthews, H. E. 1994, *A&A*, 285, 551

- Vural, J., Kreplin, A., Kishimoto, M., et al. 2014, A&A, 564, A118
- Waters, L. B. F. M., & Waelkens, C. 1998, ARA&A, 36, 233
- Weidenschilling, S. J 1997, Icarus, 127, 290
- White, J. A., Boley, A. C., Macgregor, M. A., et al. 2018, MNRAS, 474, 4500
- Zhang, K., Bergin, E. A., Blake, G. A., et al. 2016, ApJ, 818, L16
- Zhu, Z., & Waelkens, J. M. 2014, ApJ, 795, 53